

Spin fine-structure reveals bi-exciton geometry in an organic semiconductor

K.M. Yunusova,¹ S.L. Bayliss^{†,1} T. Chanelière,^{2,3} V. Derkach,⁴ J. E. Anthony,⁵ A.D. Chepelianskii,¹ and L. R. Weiss^{†6}

¹*LPS, Univ. Paris-Sud, CNRS, UMR 8502, F-91405, Orsay, France*

²*Laboratoire Aimé Cotton, CNRS, Univ. Paris-Sud,*

ENS-Cachan, Université Paris-Saclay, 91405, Orsay, France

³*Univ. Grenoble Alpes, CNRS, Grenoble INP, Institut Néel, 38000 Grenoble, France*

⁴*O. Ya. Usikov Institute for Radiophysics and Electronics of NAS of Ukraine 12, Acad. Proskury st., Kharkov, 61085, Ukraine*

⁵*Department of Chemistry, University of Kentucky, Lexington, KY 40506-0055, USA*

⁶*Cavendish Laboratory, J. J. Thomson Avenue, University of Cambridge, Cambridge CB3 0HE, UK*

In organic semiconductors, bi-excitons are key intermediates in carrier-multiplication and exciton annihilation. Their local geometry governs their electronic properties and yet has been challenging to determine. Here, we access the structure of the recently discovered $S = 2$ quintet bi-exciton state in an organic semiconductor using broadband optically detected magnetic resonance. We correlate the experimentally extracted spin structure with the molecular crystal geometry to identify the specific molecular pairings on which bi-exciton states reside.

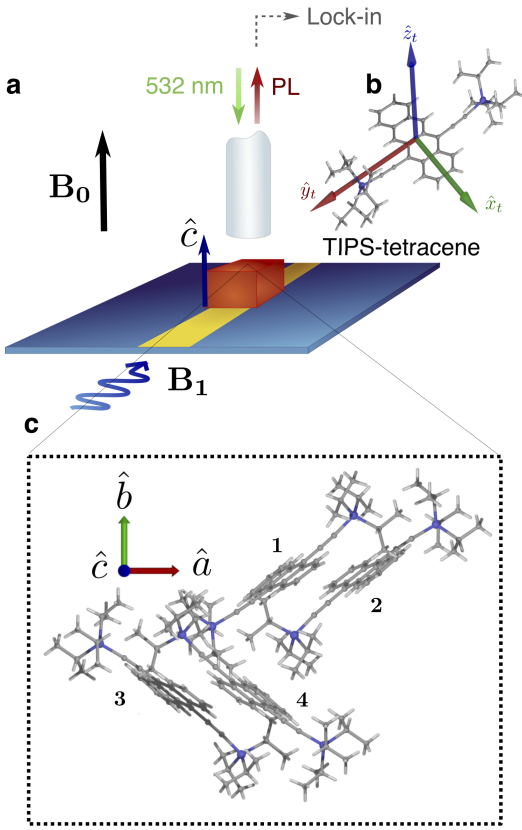


Figure 1. Broadband ODMR of triplet-pair states.

(a) Experimental schematic. Crystalline samples of TIPS-tetracene (oriented with \hat{c} -axis as shown) were optically illuminated under amplitude-modulated microwave excitation (B_1) using a broadband strip-line in liquid helium (4 K). Photoluminescence was collected via optical fibre to detect the microwave-induced change in photoluminescence (PL) as a function of both microwave frequency and static magnetic field (B_0) with $B_0 \perp B_1$. (b) Molecular structure of TIPS-tetracene and corresponding principal axes of the intra-triplet dipolar interaction ($\hat{x}_t, \hat{y}_t, \hat{z}_t$). (c) Solid-state crystal structure of TIPS-tetracene with four rotationally inequivalent molecules per unit cell labelled 1-4 and unit cell axes ($\hat{a}, \hat{b}, \hat{c}$).

Bi-excitons are key excited-state species in a range of nano-structured materials from quantum-confined inorganic systems [1–3] to synthetic molecular structures [4–6]. In organic semiconductors the exciton-pair is an intermediate in both the process of singlet fission [7–9] – the formation of a pair of spin-1 (triplet) excitons from an initial spin-0 (singlet) excitation – and its reverse process, triplet-triplet annihilation [10]. While singlet fission is of particular interest for photovoltaics [11–13], where it has been shown to increase efficiencies of solar energy harvesting beyond traditional limits [14, 15], triplet-triplet annihilation is of interest for spectral light conversion [10, 16], catalysis [17, 18], photovoltaics [16, 19], and bio-imaging [20, 21].

Despite their importance, the wavefunction of these transient, intermediate pairs remains challenging to probe. Purely optical characterization of bi-excitons can be ambiguous as their optical signatures typically overlap with those of singly-excited states. Spin resonance has played a key role in showing, unexpectedly, that in several molecular systems, singlet fission produces a long-lived bi-exciton [22–24]. An unambiguous signature of bi-exciton formation is the dominant exchange interaction between the triplets within a pair (parametrized by $J \gtrsim \text{THz}$) [23, 25]. This exchange interaction separates the pure singlet ($S = 0$) from the triplet ($S = 1$) and quintet ($S = 2$) pairings of the bi-exciton by hJ and $3hJ$ respectively and is identified via spin resonance or magneto-optic spectroscopy [25, 26].

Following identification of these bi-exciton states [23, 25], we can now investigate where such bound pairs reside. Conveniently, the $\sim \text{MHz-GHz}$ spin fine structure of the bi-exciton is determined by inter- and intra-triplet dipolar interactions and therefore provides a native probe of its spatial confinement and orientation [27, 28]. We apply this approach in TIPS-tetracene (Fig. 1b), a solution-processable singlet fission material of interest for its high singlet fission efficiency [29, 30]. TIPS-tetracene is structured with side-chain modification of the canonical fission

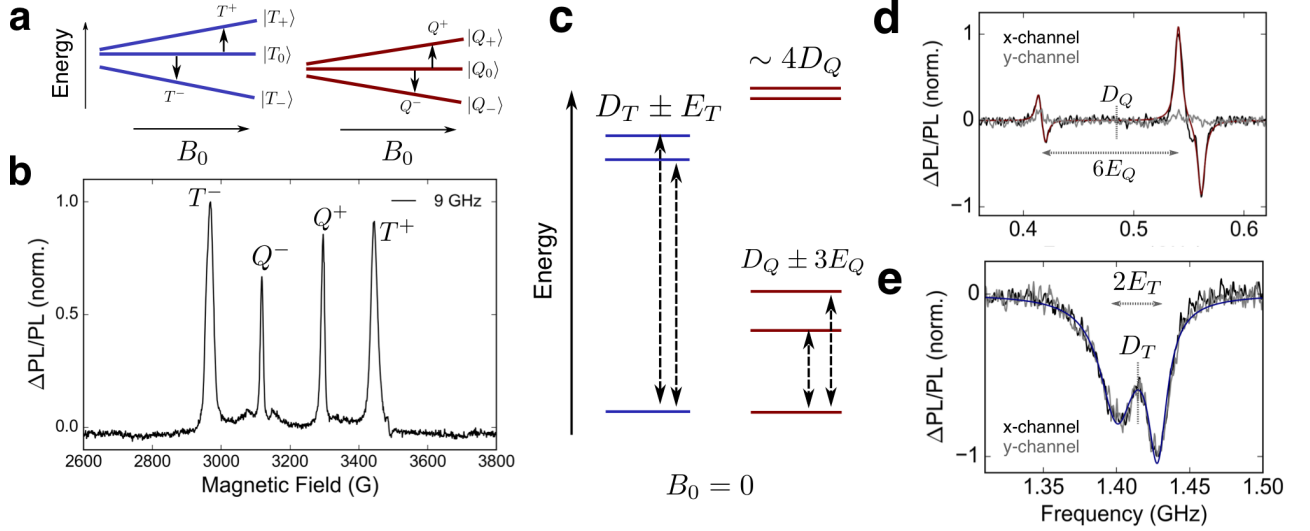


Figure 2. Field-swept and zero-field ODMR of the triplet pair state.

(a) Energy levels of the triplet and quintet $m = 0, \pm 1$ sub-levels as a function of field with transitions at 9 GHz marked with arrows to correspond to experimentally observed transitions in (b). (b) ODMR spectrum at 9 GHz showing inner quintet transitions (Q^\pm) and the outer triplet transitions (T^\pm). (c) Energy level diagram of triplet and quintet zero-field spin sub-levels. Zero-field ODMR spectra with quintet transitions (d) marked with corresponding zero-field splitting parameters (D_Q, E_Q) and simulation in red and triplet transitions (e) marked with corresponding triplet parameters (D_T, E_T) and simulations in blue.

molecule, tetracene [9]. It crystallizes with four orientationally inequivalent molecules per unit cell (Fig. 1c) yielding six possible nearest-neighbor pair-sites within a unit cell in addition to non-crystalline defect sites on which bi-excitons could reside. Here we measure the spin fine structure in TIPS-tetracene and use it to determine the molecular pair-sites where bi-excitons reside.

The fine structure is described by the following *zero-field splitting* (ZFS) Hamiltonian

$$\hat{H}_{zfs}/h = \mathbf{S}^\top \cdot \mathbf{D} \cdot \mathbf{S} = D(\hat{S}_z^2 - \frac{1}{3}S(S+1)) + E(\hat{S}_x^2 - \hat{S}_y^2) \quad (1)$$

where \mathbf{D} is the dipolar tensor (D -tensor) with parameters D, E and \mathbf{S} is the relevant vector of spin operators (with total spin $S = 1, 2$ for triplet, quintet states) defined along the principal axes ($\hat{x}, \hat{y}, \hat{z}$) of the D -tensor.

We now show how the quintet fine-structure (D_Q, E_Q and the principal axes $\hat{x}_q, \hat{y}_q, \hat{z}_q$) depends on the underlying triplet pair orientation on two molecules (labeled here a and b). We assume that each triplet has the same zero-field parameters (D_T, E_T) and differ only in orientation and position. We define the principal axes of the first triplet state as $(\hat{x}_a, \hat{y}_a, \hat{z}_a)$ and the second triplet as $(\hat{x}_b, \hat{y}_b, \hat{z}_b)$, defined relative to the molecular structure as in Fig. 1b with the vector between them given by \vec{r}_{ab} and unit vector $\hat{u}_{ab} = \vec{r}_{ab}/|\vec{r}_{ab}|$. The zero-field Hamiltonian of the pair in the uncoupled basis is then given by

$$\hat{H}_{zfs}^{(1\otimes 1)}/h = \sum_{i=a,b} \mathbf{S}_i^\top \cdot \mathbf{D}_T^i \cdot \mathbf{S}_i - \Gamma(\hat{u}_{ab} \cdot \mathbf{S}_a)(\hat{u}_{ab} \cdot \mathbf{S}_b) + J\mathbf{S}_a \cdot \mathbf{S}_b \quad (2)$$

where $\Gamma = \frac{3\mu_0\mu_B^2 g^2}{4\pi|\vec{r}_{ab}|^3}$ gives the strength of the inter-triplet dipolar interaction with μ_0 the magnetic permeability of free-space, μ_B the Bohr magneton, and g the g-factor. In the limit of strong exchange coupling ($J \gg D_T$), the Hamiltonian is approximately diagonal in the coupled spin basis defined by the states of pure total spin [25, 26, 31]. Converting the above Hamiltonian to the coupled basis and projecting into the $S = 2$ subspace gives the quintet zero-field fine-structure Hamiltonian as

$$\hat{H}_{zfs}^{(2)}/h = \mathbf{S}^\top \cdot \mathbf{D}_Q \cdot \mathbf{S} \quad (3)$$

where $\mathbf{S} = (\hat{S}_x, \hat{S}_y, \hat{S}_z)$ are the Pauli spin operators for total spin-2. The quintet zero-field tensor \mathbf{D}_Q in terms of the underlying triplet fine structure, inter-triplet distance and dipolar interaction is given by

$$\mathbf{D}_Q = \frac{D_T}{6} \left(\sum_{i=a,b} \hat{z}_i \hat{z}_i^\top - \frac{2}{3} \hat{I}_3 \right) + \frac{E_T}{6} \sum_{i=a,b} (\hat{x}_i \hat{x}_i^\top - \hat{y}_i \hat{y}_i^\top) - \frac{\Gamma}{3} (\hat{u}_{ab} \hat{u}_{ab}^\top - \frac{1}{3} \hat{I}_3) \quad (4)$$

where \hat{I}_3 is the identity matrix in three dimensions (a detailed derivation is in the Supplemental Material [32]). Converting $\hat{H}_{zfs}^{(2)}$ to the form of Eq. 1 yields the quintet dipolar parameters D_Q, E_Q , and the principal axes $\hat{x}_q, \hat{y}_q, \hat{z}_q$ (the eigenvectors of \mathbf{D}_Q).

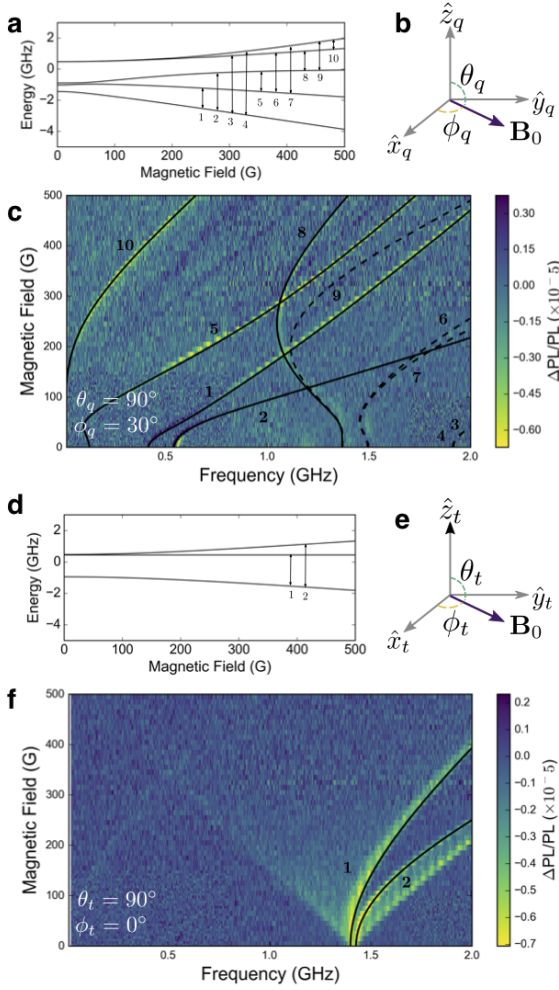


Figure 3. Fine-structure tensors from broadband ODMR. (a,d) Energy level diagram for the quintet (a) and triplet (d) states as a function of magnetic field. Arrows indicate potential transitions, corresponding to lines in (c) and (f) respectively. (b,e) Schematic representation of the orientation of \mathbf{B} in the quintet (b) and triplet (e) fine-structure axes. (c) ODMR transitions associated with the quintet state with overlay of simulated transitions. Signal has been isolated by subtracting a scaled out-of-phase (Y)-channel signal from the in-phase signal to remove triplet contributions. Black lines show simulations given for $\theta_q = 90^\circ$ and $\phi_q = 30^\circ$ with an uncertainty of $\pm 5^\circ$ where solid (dashed) lines overlay (un-)observed transitions. (f) Y-channel (out-of-phase) ODMR map of the triplet state with overlay of calculated transitions in black with $\theta_t = 90^\circ$ and $\phi_t = 0$.

Each distinct potential pair site can be identified by its unique fine structure parameters in a single crystal with the relation given by Eq. 4. With this motivation we use a macroscopic crystal (\sim mm-scale single-crystalline domain) and measure the principal values and axes of the D -tensors of the triplet and quintet states using broadband optically detected magnetic resonance (ODMR). The experimental setup is shown in Fig. 1a and includes 532 nm continuous-wave (CW) light excita-

tion, static magnetic field (\mathbf{B}_0), and microwave radiation (\mathbf{B}_1) with variable frequency delivered through a broadband copper strip-line. The TIPS-tetracene crystal is aligned with $\mathbf{B}_0 \parallel \hat{c}$. The ODMR signal is measured by lock-in detection of microwave-induced changes in photoluminescence (PL).

We first perform fixed-frequency (9 GHz), field-swept ODMR. In agreement with previous measurements using transient electron spin resonance, we observe two pairs of spin-transitions consistent with the $\Delta m = \pm 1$ transitions of the $S = 1$ triplet exciton (which we label T^\pm) and the $\Delta m = \pm 1$ transitions of the $S = 2$ quintet state (labeled Q^\pm), as shown in the Fig. 2a,b. (Note that this spectrum confirms the expected orientation of the crystal aligned with $\mathbf{B}_0 \parallel \hat{c}$ as noted in the Supplemental Material [32]) We correlate these observed high-field transitions with zero-field transitions (magnetic field strength $\mathbf{B}_0 = 0$, Fig. 2c,d), measured here to sensitively determine the zero-field splitting parameters. We now describe the microwave transitions observed experimentally. Two of the triplet energy levels are separated by $|hD_T|$ from the lowest level, and the two upper eigenstates are further split by $|2E_T h|$ (Fig. 2c in blue). ODMR then occurs at microwave frequencies $\nu = D_T \pm E_T$. The three lowest quintet levels are split by $|D_Q|$ from the ground state to the first two states with a further splitting of $|6E_Q|$ between those two upper levels (Fig. 2c in red). This leads to ODMR transition frequencies at $\nu = D_Q \pm 3E_Q$. Note that the previously reported D -parameters for TIPS-tetracene are $D_T \sim 1.4$ GHz and $D_Q \sim D_T/3$ [23, 33].

The spectra of triplets and bi-excitons can be separated in ODMR using the difference in lifetime of the two species [23, 33]. The microwave amplitude modulation frequency (137 Hz) is chosen such that the triplet signal appears with equal amplitude on the in-phase (X-channel) and out-of-phase (Y-channel) lock-in channels, which corresponds to the inverse lifetime of the triplets. The signal from shorter lived bi-excitons appears only on the X-channel and can be isolated by subtracting X and Y channels. The zero-field X- and Y-channel ODMR spectra are plotted in Fig. 2d,e in black (X-channel) and grey (Y-channel). The transitions on the Y-channel are consistent with triplets with $|D_T| = 1.4$ GHz and $|E_T| = 14$ MHz (Fig. 2e, with overlaid spectral fit in blue). Transitions in the frequency region expected for the quintet only appear on the X-channel and give $|D_Q| = 477$ MHz and $|E_Q| = 22$ (Fig. 2d, with overlaid spectral fit in red). The measurement of the E -parameters here is made possible by the reduced linewidths observed at zero-field relative to previous measurements under non-zero magnetic field. (Note that the spectral fit in Fig. 2d includes a minor species with slightly larger quintet parameters ($|D_Q| = 490$, $|E_Q| = 24$) that quickly decays in intensity with field.)

Having extracted the principal components of the

triplet and quintet fine-structure at zero-field, we now map the resonance frequencies as a function of magnetic field to determine the corresponding orientations of the principal axes. The experimental ODMR maps for quintet and triplet states are shown in Fig. 3c,f. The observed resonances cannot be fit by a spin-1 state, which further confirms the assignment (see Supplemental Material [32]). We parametrize the orientation of the principal axes relative to the magnetic field with the polar angle θ and azimuthal angle ϕ as shown in Fig. 3b,e. The orientation of the quintet fine-structure axes is obtained by fitting these maps with the spin transitions predicted by the fine structure parameters determined at zero-field with the orientation as input. There are 10 possible transitions between the five quintet spin sub-levels (Fig. 3a), which are overlaid on the quintet ODMR map (Fig. 3c). It should be noted that the visibility of transitions depends on populations and selection rules, and transitions 3,4,6,7 and 9 are not clearly observed experimentally. The quintet state is oriented with fixed $\theta_q = 90 \pm 5^\circ$ between \hat{z}_q and \mathbf{B}_0 and $\phi_q = 30 \pm 5^\circ$ between \hat{x}_q and \mathbf{B}_0 .

The evolution of the triplet zero-field transitions (~ 1.4 GHz) with field, shown in Fig. 3f are consistent with $\theta_t = 90^\circ$ (simulated transitions shown in black). We also observe $\theta_t \sim 0$ peaks due to a weak powder background, which decays quickly with field. The dominant $\theta_t = 90^\circ$ triplet orientation correlates with the high-field spectrum (Fig. 2b): triplet peaks are separated in field by $\sim hD/g\mu_B$, which occurs when $\theta_t \sim 90^\circ$, whereas no peaks are observed for $\theta_t \sim 0$ (separation in field of $\sim 2D/g\mu_B$). Note that the transitions are consistent with $\phi_t \sim 0$, but this angle could not be extracted reliably and is not required for subsequent analysis because the triplet states are nearly axially symmetric (i.e., $E_T \approx 0$). As the D-tensor principal values and axes in the laboratory frame are obtained from a crystalline sample aligned with $\mathbf{B}_0 \parallel \hat{c}$, we can now compare them with the theoretically predicted D-tensors in the TIPS-tetracene crystal structure.

There are six potential nearest-neighbor dimer configurations in the TIPS-tetracene crystal structure (see Fig. 1c) and for each we can calculate the fine structure parameters ($D_Q, E_Q, \theta_q, \phi_q$) using Eq. (4) and the point-dipole approximation, the dipolar axes shown in Fig. 1b and the intermolecular distances extracted from the crystal structure [34]. The full set of values are summarized in the Supplemental Material [32]. The observed quintet parameters and extracted angles of $\theta_q \sim 90^\circ$ and $\phi_q \sim 30^\circ$ are consistent with exchange-coupled triplets localized on dimers with molecules 1,2 and 3,4 (labelled in Fig. 1c). The extracted local quintet fine structure is visualized in Fig. 4 where the full quintet and triplet dipolar interactions are shown with respect to the magnetic field in the lab frame and crystallographic axes, summarizing the local structure of quintet and triplet states in TIPS-tetracene and their relation to intermolecular ge-

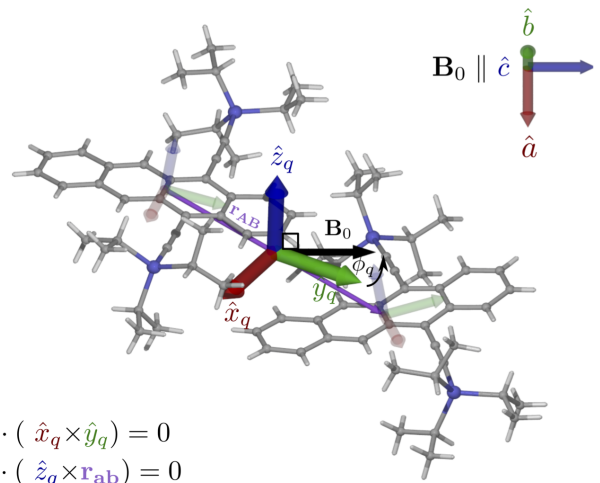


Figure 4. Local geometry of the quintet fine-structure tensor in the TIPS-tetracene crystal with an angle of $\theta_q = 91.6^\circ$ and $\phi_q = 30.6^\circ$, where the crystal is oriented with $\mathbf{B}_0 \parallel \hat{c}$ with two co-planar triads of vectors, $(\hat{x}_q, \hat{y}_q, \mathbf{B}_0)$ and $(\hat{z}_q, \mathbf{r}_{ab}, \mathbf{B}_0)$.

ometry.

We have shown how the sensitivity of broadband magnetic resonance enables identification of triplet-pair geometries in a material with many possible intermolecular configurations. This approach is broadly applicable even in cases where the crystal structure is not known or relevant (as in disordered materials and devices with trap sites). Here we find that the triplet pairs are localized on the closest π -stacked dimers of the crystal structure. As the fine structure is consistent with minimal modification from the ground-state crystal structure, these results suggest that geometric reorganization is negligible in the quintet bi-exciton excited-state. This description of the geometry of the triplet pair sets the foundation for time-resolved measurements to allow investigation of the transient localization and molecular reorganization of the pair-state. While here we have examined a singlet fission material, this technique is broadly applicable to any device architecture with interacting excited states, from those incorporating two-dimensional materials and quantum dots to emerging hybrid organic-inorganic and bio-engineered structures.

Acknowledgements We are thankful for insightful discussions with H. Bouchiat and R.H. Friend and acknowledge support from ANR SPINEX and Labex ANR-10-LABX-0039-PALM. L.R. Weiss acknowledges support from Clare College, Cambridge. The authors declare no competing financial interests. Correspondence should be addressed to A.D.C. (chepelianskii@lps.u-psud.fr) and L.R.W. (lrweiss@uchicago.edu).

[†]Present address: Pritzker School of Molecular Engineering, University of Chicago, Chicago, Illinois 60637, USA.

-
- [1] G. W. Bryant, Phys. Rev. B **41**, 1243 (1990).
- [2] G. Chen, T. Stievater, E. Batteh, X. Li, D. Steel, D. Gammon, D. Katzer, D. Park, and L. Sham, Phys. Rev. Lett. **88**, 117901 (2002).
- [3] Y. Hu, S. Koch, M. Lindberg, N. Peyghambarian, E. Pollock, and F. F. Abraham, Phys. Rev. Lett. **64**, 1805 (1990).
- [4] M. A. Baldo, C. Adachi, and S. R. Forrest, Phys. Rev. B **62**, 10967 (2000).
- [5] V. Klimov, D. McBranch, N. Barashkov, and J. Ferraris, Phys. Rev. B **58**, 7654 (1998).
- [6] K. Masui, H. Nakanotani, and C. Adachi, Org. Electron. **14**, 2721 (2013).
- [7] M. B. Smith and J. Michl, Chem. Rev. **110**, 6891 (2010).
- [8] S. Singh, W. Jones, W. Siebrand, B. Stoicheff, and W. Schneider, J. Chem. Phys. **42**, 330 (1965).
- [9] C. Swenberg and W. Stacy, Chem. Phys. Lett. **2**, 327 (1968).
- [10] T. N. Singh-Rachford and F. N. Castellano, Coord. Chem. Rev. **254**, 2560 (2010).
- [11] A. Rao and R. H. Friend, Nat. Rev. Mater. **2**, 17063 (2017).
- [12] M. Hanna and A. Nozik, J. Appl. Phys. **100**, 074510 (2006).
- [13] M. J. Tayebjee, A. A. Gray-Weale, and T. W. Schmidt, J. Phys. Chem. Lett. **3**, 2749 (2012).
- [14] M. Einzinger, T. Wu, J. F. Kompalla, H. L. Smith, C. F. Perkinson, L. Nienhaus, S. Wiegold, D. N. Congreve, A. Kahn, M. G. Bawendi, *et al.*, Nature **571**, 90 (2019).
- [15] D. N. Congreve, J. Lee, N. J. Thompson, E. Hontz, S. R. Yost, P. D. Reusswig, M. E. Bahlke, S. Reineke, T. Van Voorhis, and M. A. Baldo, Science **340**, 334 (2013).
- [16] Y. Y. Cheng, T. Khoury, R. G. Clady, M. J. Tayebjee, N. Ekins-Daukes, M. J. Crossley, and T. W. Schmidt, Phys. Chem. Chem. Phys. **12**, 66 (2010).
- [17] B. D. Ravetz, A. B. Pun, E. M. Churchill, D. N. Congreve, T. Rovis, and L. M. Campos, Nature **565**, 343 (2019).
- [18] R. S. Khnayzer, J. Blumhoff, J. A. Harrington, A. Haeefe, F. Deng, and F. N. Castellano, Chem. Commun. **48**, 209 (2012).
- [19] V. Gray, D. Dzebo, M. Abrahamsson, B. Albinsson, and K. Moth-Poulsen, Phys. Chem. Chem. Phys. **16**, 10345 (2014).
- [20] Q. Liu, T. Yang, W. Feng, and F. Li, J. Am. Chem. Soc. **134**, 5390 (2012).
- [21] Q. Liu, M. Xu, T. Yang, B. Tian, X. Zhang, and F. Li, ACS Appl. Mater. Interfaces **10**, 9883 (2018).
- [22] M. J. Tayebjee, S. N. Sanders, E. Kumarasamy, L. M. Campos, M. Y. Sfeir, and D. R. McCamey, Nat. Phys. **13**, 182 (2017).
- [23] L. R. Weiss, S. L. Bayliss, F. Kraffert, K. J. Thorley, J. E. Anthony, R. Bittl, R. H. Friend, A. Rao, N. C. Greenham, and J. Behrends, Nat. Phys. **13**, 176 (2017).
- [24] D. Lubert-Perquel, E. Salvadori, M. Dyson, P. N. Stavrinou, R. Montis, H. Nagashima, Y. Kobori, S. Heutz, and C. W. Kay, Nat. Commun. **9**, 4222 (2018).
- [25] S. L. Bayliss, L. R. Weiss, A. Mitoglu, K. Galkowski, Z. Yang, K. Yunusova, A. Surrente, K. J. Thorley, J. Behrends, R. Bittl, *et al.*, Proc. Natl. Acad. Sci. USA **115**, 5077 (2018).
- [26] S. L. Bayliss, L. R. Weiss, A. Rao, R. H. Friend, A. D. Chepelianskii, and N. C. Greenham, Phys. Rev. B **94**, 045204 (2016).
- [27] J. A. Weil and J. R. Bolton, *Electron paramagnetic resonance: elementary theory and practical applications* (John Wiley & Sons, 2007).
- [28] H. Benk and H. Sixl, Mol. Phys. **42**, 779 (1981).
- [29] H. L. Stern, A. Cheminal, S. R. Yost, K. Broch, S. L. Bayliss, K. Chen, M. Tabachnyk, K. Thorley, N. Greenham, J. M. Hodgkiss, *et al.*, Nat. Chem. **9**, 1205 (2017).
- [30] H. L. Stern, A. J. Musser, S. Gelinis, P. Parkinson, L. M. Herz, M. J. Bruzek, J. Anthony, R. H. Friend, and B. J. Walker, Proc. Natl. Acad. Sci. USA **112**, 7656 (2015).
- [31] T. Yago, K. Ishikawa, R. Katoh, and M. Wakasa, J. Phys. Chem. C **120**, 27858 (2016).
- [32] See Supplemental Material at [URL will be inserted by publisher].
- [33] S. L. Bayliss, A. D. Chepelianskii, A. Sepe, B. J. Walker, B. Ehrler, M. J. Bruzek, J. E. Anthony, and N. C. Greenham, Phys. Rev. Lett. **112**, 238701 (2014).
- [34] D. Eaton, S. Parkin, and J. Anthony, CCCDC (2013), 10.5517/cc119qsv.